Impacts of Extreme Climate on Australia's Green Cover (2003-2018): A MODIS and Mascon Probe

A. Saleem[a], J.L, Awange[a,b], M. Kuhn[a], B. John[a], K. Hu[a]

[a] *School of Earth and Planetary Science, Spatial Science Discipline, Curtin University, Perth, Australia*
[b] *Geodetic Institute, Karlsruhe Institute of Technology, Engler-Strasse 7, D-76131, Karlsruhe, Germany*

Abstract

Australia as a continent represents a semi-arid environment that is generally water-limited. Changes in rainfall pattern will inevitably occur due to rising temperatures caused by climate change, which has a direct impact on the distribution of Australia's vegetation (green cover). As variability in rainfall continues to increase, i.e., in frequency and/or magnitude, due to climate change, extreme climate events such as droughts are predicted to become more pervasive and severe that will have an adverse effect on vegetation. This study investigates the effects of extreme climate on Australia's green cover during 2003-2018 for the end of rainy seasons of April and October in the northern and southern parts, respectively, to (i) determine the state of vegetation and its changes, (ii) identify "hotspots", i.e., regions that constantly experienced statistically significant decrease in NDVI, and (iii), relate changes in the identified hotspots to GRACE-hydrological changes. These are achieved through the exploitation of the statistical tools of Principal Component Analysis (PCA) and Mann-Kendel Test on Gravity Recovery and Climate Experiment (GRACE) hydrological products on the one hand, and the utilization of Australia's rainfall product and Moderate Resolution Imaging Spectroradiometer Normalized Difference Vegetation Index (MODIS-NDVI) used here with its native spatial resolution of $0.002413° \times 0.002413°$ on the other hand. Differences between 3-year intervals from 2003 to 2018 for both April and October datasets are used to quantify vegetation variations. Through area change analysis, the vegetation differences (2003-2018) indicate that April exhibited larger increase (13.77% of total vegetation area) than decrease (7.83%) compared to October, which experienced slightly larger decrease (9.41%) than increase (8.71%). South Australia and Western Australia emerge as "hotspots" in which vegetation statistically decreased in October, with no noticeable change in April. GRACE-based hydrological changes in both hotspots reflect a decreasing trend (2003-2009) and increasing trend (2009-2012) that peaks in 2011, which then

transitions towards a gradually decreasing trend after 2012. Australia-wide climate variability (ENSO and IOD) influenced vegetation variations during the data period 2003 to 2018.

Keywords: Extreme climate; Vegetation change; NDVI; Australia; Climate variability

1. Introduction

Extreme climate events, such as droughts and floods, are predicted to become more frequent and severe because of changes in climate variability (Ma et al., 2015). Drought events alone are projected to increase within most African nations, southern Europe, the Middle East, the Americas, Australia, and South East Asia (Ponce-Campos et al., 2013). Rainfall patterns affected by climate variability exacerbate drought and flood events (Ma et al., 2015; Van Dijk et al., 2013; Murthy et al., 2016, 2017), which is significant towards vegetation dynamics and productivity, as approximately 50% of the terrestrial vegetation productivity across the world is dependent directly upon the availability of water (Yang et al., 2014). Previous studies have demonstrated that extreme climate events have a profound effect towards vegetation dynamics and productivity. For example, large scale vegetation losses were recorded during the aftermath of the 2005 and 2010 droughts within the Amazon basin (Lewis et al., 2011). In Africa, mass agricultural drought from 1981 to 2010 caused famine emergencies across the nations that resulted in more than half a million deaths (Rojas et al., 2011; Mpelasoka et al., 2018; Awange et al., 2016). In Australia, the "Millennium Drought", which affected agriculture, lasted from 2001 to 2009, and is estimated to have resulted in a loss of 1.6% of Australian GDP (Gross Domestic Product) between 2002 and 2003 (Van Dijk et al., 2013). Future projected drought events are likely to have an adverse effect on vegetation (Pan et al., 2018). Monitoring of vegetation productivity, therefore, is essential for understanding climate variability's impacts on terrestrial ecosystem (Chen et al., 2014), thereby contributing towards informing governmental policies on managing resources to alleviate negative effects.

Satellite remote sensing provides an alternate, quicker and more cost-effective method as opposed to on-ground surveys to obtain data regarding vegetation productivity over time and space at a regional and global scale through the measure of vegetation indices (VI) over terrestrial ecosystems (Chen & Gillieson, 2009; Lu et al., 2003; Zhang et al., 2003). Vegetation indices provide integrated information regarding the measure of green leaf area, structure and vegetation chlorophyll content (Ma et al., 2015). Remotely sensed VI data can come from the

Moderate Resolution Imaging Spectroradiometer (MODIS) sensor that is able to provide data with very little influence from other variables such as land conditions, water vapour and lower-cloud contamination (Zhang et al., 2003; Broich et al., 2014; Huete et al., 2010). Waring et al. (2006) determined that MODIS enhanced vegetation index (EVI) values at a spatial resolution of 1-km provide similar information to values derived from localized field sampling, i.e., areal averages of in-situ data were comparable with the 1-km MODIS resolution as measured by correlations between MODIS EVI and field survey data of tree richness in eco-regions across the contiguous U.S.A. In other examples, Tomar et al. (2014) and Pandey et al. (2015) employed MODIS NDVI products in the study of rice equivalent yield, while Zhang et al. (2003) utilized them to monitor vegetation phenology on an area located in New England, USA, and concluded that the results obtained from their investigation were both geographically and ecologically consistent with the pattern of vegetation transition behaviour in the region determined by previous field-based studies. These studies demonstrate that the MODIS sensors are able to provide an adequate and meaningful measure of vegetation across a large surface area. However, MODIS NDVI data is taken at a rather coarse resolution (e.g. 250 m, 500 m, and 1000 m), in which each pixel within the remotely sensed data represents a combined response of diverse species that may have different vegetation activities (Zhang et al., 2017). In terms of analysing vegetation productivity at a continental scale, this weakness can be disregarded as the overall vegetation is the variable of interest as opposed to specific species.

Australia as a continent represents a semi-arid environment that is generally water-limited (Donohue et al., 2009; Hu et al., 2019), as dryland is estimated to encompass approximately 80% of Australia's land surface (Broich et al., 2014). Australia's vegetation is depended upon a series of factors such as rainfall, topography, soil type and fertility, and climate (Hughes , 2011). Remote sensing study of vegetation dynamics over time and its relation to climate variability and extreme climate events have been extensively documented within Australia. For example, in a study to understand vegetation response to altered hydro-climatic conditions over time, Yang et al. (2014) examined the effects of hydrological controls on the variability in surface vegetation greenness over the periods of 1982-2010 and discovered a strong association between remotely sensed NDVI anomalies and monthly total water storage anomalies, concluding that total water storage data is a superior indicator for variability of surface vegetation than precipitation. In a separate study that measured vegetation growth over time, Donohue et al. (2009) examined the response of different vegetation functional types, i.e., non-deciduous perennial vegetation types, deciduous, annual and ephemeral vegetation types, towards changing climatic conditions using vegetation data sourced from the Advanced Very High-Resolution Radiometer (AVHRR) instrument and discovered an 8% increase in vegetation growth of primarily persistent woody species across the north and north-east of Australia for 1981-2006. During a period that included extreme drought and wet years, Broich et al. (2014) investigated the relationship between surface vegetation phenology and climate variability for the period 2000-2013 by utilizing MODIS NDVI data and found results consistent with Donohue et al. (2009) in which areas of vegetation productivity affected by long term drought increased over time in most of eastern Australia. On a regional scale, Ma et al. (2015) studied vegetation dynamics and phenology using MODIS NDVI in south-eastern Australia between 2000 and 2014 to examine the impact of the Millennium Drought that lasted from 2001 to 2009. Their study revealed that there are dramatic impacts of drought and wet extremes on vegetation dynamics for south-eastern Australia, and furthermore, drought resulted in widespread reductions and to some extend collapse in the normal patterns of seasonality. Finally, in many cases during the drought years, there was no detectable phenological cycle, which significantly affects Australia's role as a prominent global carbon sink source.

The studies discussed above demonstrate the efficiency and adequacy of remotely sensed data to monitor vegetation productivity over a large area through time (see e.g., Jiao et al. (2020)). However, studies of vegetation productivity over time have been performed with altered spatial resolution by re-scaling and re-sampling raw data of higher spatial resolutions. For example, Andrew et al. (2017) re-sampled their Global Inventory Modelling and Mapping Studies (GIMMS)-3g NDVI data ($0.25°$ by $0.25°$) to a larger scale of $0.9°$ by $0.9°$ in order to match with Gravity Recovery and Climate Experiment (GRACE) data resolution of the same time period. Yang et al. (2014) also used GIMMS 3g NDVI data in their study that was re-sampled to $1° \times 1°$ in accordance to the GRACE data resolution. Donohue et al. (2009) re-sampled vegetation data from $0.01° \times 0.01°$ to $0.08°$. Ma et al. (2015) re-sampled MODIS EVI resolution of $0.05°$ to $0.5°$ to match the resolution of the Standardized Precipitation and Evapotranspiration Index (SPEI) drought severity data. The process of re-sampling remotely sensed vegetation data results in increased errors in land and vegetation cover (Andrew et al., 2017). Maintaining the native resolution of used data ensures that the integrity of the vegetation status is not compromised. To this end, this study employs the Earth Resources Observation and Science (EROS) Moderate Resolution Imaging Spectroradiometer (eMODIS) Normalized Difference Vegetation Index

(NDVI) V6 data at its native spatial resolution ($0.002413° \times 0.002413°$) rarely used before to investigate the effects of extreme climate on Australia's green cover during 2003-2018 for the end of rainy season months of April and October for northern and southern regions of Australia, respectively. These months are chosen due to the fact that vegetation is considered to have utilised the rain water, and as such, the green cover are at their maximum. In particular, the study aims to (i) determine the state of vegetation and its changes, (ii) identify "hotspots", i.e., regions that constantly experienced statistically significant decrease in NDVI, and (iii), relate the changes in these hotspots to Gravity Recovery and Climate Experiment (GRACE) derived hydrological changes and Australia-wide rainfall. These aims are achieved using statistical tools of Principal Component Analysis (PCA) and Mann-Kendel Test.

The remainder of the study is presented as follows. In section 2, Australia-wide vegetation variability and its primary drivers in response to rainfall are briefly discussed. Description of the different data that are utilized in this study is also included within section 2. Section 3 provides an overview of the pre-processing and analysis methods that are employed while Section 4 presents and discusses the results. Section 5 summaries the main outcomes of the study.

2. Study area and Data

2.1. Australia's vegetation in relation to rainfall

Australia comprises of an area of approximately 7.6 million km^2 (Figure 1) and is exposed to a wide range of climate varying over different regions (Broich et al., 2014; Fleming et al., 2010; Fleming & Awange, 2013). As it is a semi-arid environment with most of its area classified as drylands (i.e., 80%) (Broich et al., 2014), the amount of precipitation received in Australia is stated to be lower than other inhabited continents (Forootan et al., 2016). 80% of Australia's land surface receive an average annual precipitation that rarely exceeds 600 mm while 50% of the land surface experience less than 300 mm on average (Broich et al., 2014). The north of Australia is recorded to have the majority of precipitation occurring during the summer season (December-February) while the south and southwest of the country encounters major rainfall during the winter season (June-August) (King et al., 2014; Awange et al., 2009, 2011; Rieser et al., 2010). The El Niño-Southern Oscillation (ENSO) and the Indian Ocean Dipole (IOD) are known to be the primary drivers in Australia's inter- and intra-annual variability of rainfall (Forootan et al., 2016; King et al., 2014). During formulation of ENSO events, La Niña events are associated with increased rainfall particularly in the northern and eastern regions of Australia whereas El Niño events cause the opposite to occur, promoting reduced rainfall within these regions as well as drought occurrences within the interior of Australia. For the western and southern regions of Australia, IOD is known to be the primary driver of rainfall as negative IOD events are recorded to induce increased precipitation over these areas, which in conjunction with La Niña events, causes considerable precipitation to occur (Forootan et al., 2016). These drivers of rainfall influence the vegetation distribution Australia-wide (Hughes , 2011). Forest species occur primarily in high rainfall areas of the country, whereas the arid and semi-arid interior that receive scarce precipitation is dominated by shrubs, desert vegetation, and grassland. Vegetation in the northern region of Australia is dominated by a savanna ecosystem that consist of mixed woodland and grassland (Broich et al., 2014).

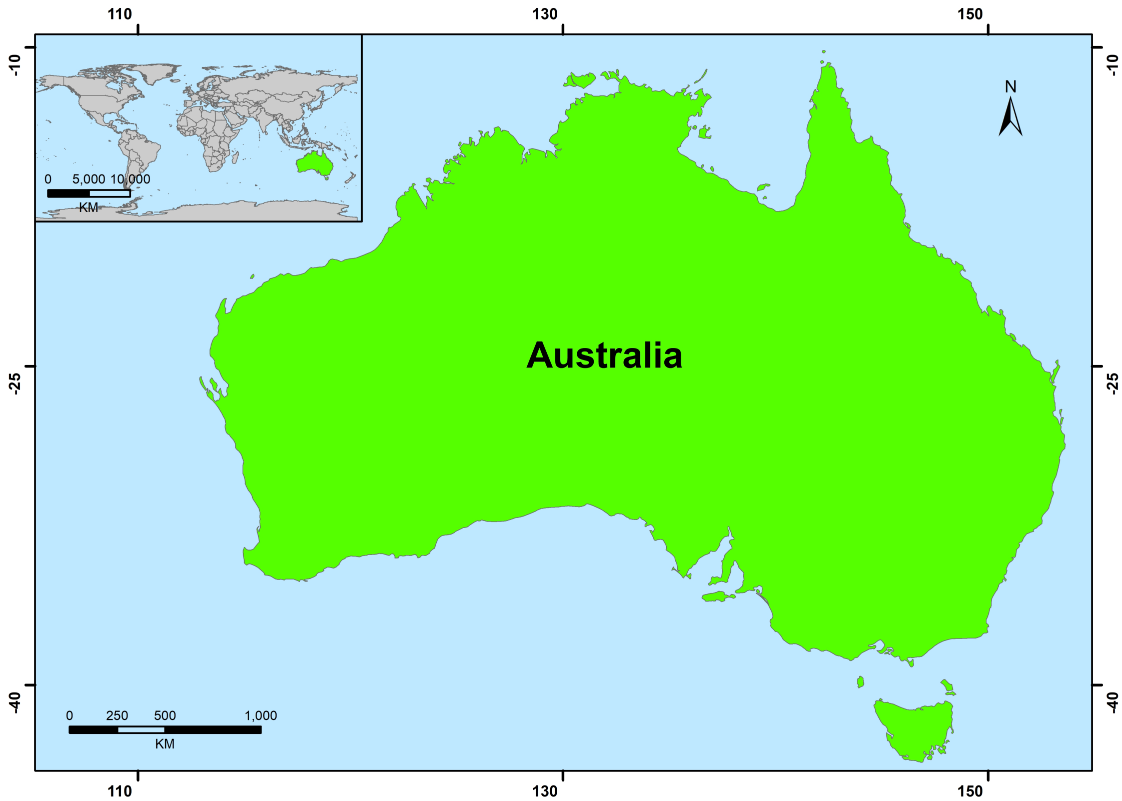

Figure 1: Inset: Location map of Australia in relation to entire world. The main map is the boundary of study area, i.e., Australia-wide.

2.2. MODIS Normalized Difference Vegetation Index (NDVI) data

The Earth Resources Observation and Science (EROS) Data Archive for vegetation monitoring - EROS Moderate Resolution Imaging Spectroradiometer (eMODIS) collection is used for this study. This collection is based on MODIS data acquired by the National Aeronautics and Space Administration (NASA) Earth Observing System (EOS). The eMODIS data are generally provided in two forms; 7 as well as 10 days composites for NDVI and reflectance using the AQUA MODIS sensor. As the 7 days eMODIS products and reflectance are available only over continental US, for this study, the 10 days NDVI (know as eMODIS NDVI V6) products are downloaded from the United States Geological Survey (USGS) Earth Explorer database (https://earthexplorer.usgs.gov/) at it's highest (native) spatial resolution of $0.002413^\circ \times 0.002413^\circ$ (250 m x 250 m). These products are developed by eMODIS specifically to overcome issues of re-projection, file format, and sub-setting of MODIS data, i.e., MOD13A1-NDVI, MOD13Q1-NDVI, and other available products for vegetation studies. The downloaded eMODIS NDVI V6 datasets (2003-2018) used for this study include the calender periods of the first 10 days, i.e., 1-10, for April and October months, respectively, representing the end of rainy seasons for Australia's southern and northern regions.

2.3. GRACE-Mascon's Total Water Storage Anomaly data

Gravity Recovery and Climate Experiment (GRACE) satellites launched in 2002 (Tapley et al., 2004) operated until 2017 where a follow-on mission was launched. It measures changes in total water storage (TWS; surface water, groundwater, soil moisture, ice/snow and vegetation water). Here, the GRACE-mascon (mass concentration) TWS data from NASA's Jet Propulsion Laboratory (JPL) available through the Colorado Centre for Astrodynamics Research (CCAR; `https://podaac.jpl.nasa.gov/GRACE`) is employed to infer changes in soil moisture relevant to vegetation growth with the assumption that changes in surface, groundwater, ice/snow, and vegetation water over the hotspots are negligible, and as such, the major changes noticeable in TWS are due to soil moisture. Indeed, the potential of GRACE-TWS to indicate vegetation variability has been demonstrated, e.g., in (Andrew et al., 2017; Ndehedehe et al., 2019; Tao et al., 2020). This study, therefore, utilizes gridded Total Water Storage Anomaly (TWSA) data at a spatial resolution of $3^{\circ} \times 3^{\circ}$ retrieved from the online mascon visualization tool developed by the University of Colorado, Boulder. Compared to other vegetation indicators such as those from MODIS and GLDAS, GRACE's TWS for the period 2003-2018 are readily obtained from the mascon visualization tool at spatial resolution targeting hotspot areas over Australia without further calculations. A Coastline Resolution Improvement (CRI) filter has been applied to the mascons cells during post-processing to separate land signals from ocean signals within the same cells. The monthly TWS data examined for this study are mascon cells that coincides with the identified hotspot areas.

2.4. Bureau of Meteorology (BoM) Rainfall Data

Australia-wide rainfall data is sourced from the Australia government's Bureau of Meteorology (BoM) website (`www.bom.gov.au`) at a $0.05^{\circ} \times 0.05^{\circ}$ monthly spatio-temporal resolution. The BoM rainfall product is stated to be the most reliable rainfall product in Australia that is generated by interpolating rain-gauge stations across Australia (Awange et al., 2019). For the purpose of this study, a principal component analysis (PCA) of Australia-wide rainfall data over the study period 2003-2018 is undertaken and used for evaluating the rainfall variability over the identified hotspots.

3. Methods

3.1. MODIS NDVI Data Pre-Processing

The eMODIS NDVI V6 datasets are clipped using a continental Australia shapefile sourced from the Department of Agriculture and Water Resources to restrict the area extent to mainland Australia and the island of Tasmania (Figure 1). A study by Xiao et al. (2002) stated that a threshold of ≥ 0.25 of NDVI values is appropriate to define healthy vegetation coverage in the northern latitudes. Although this threshold is specified for the northern latitudes, Newnham et al. (2011) found changes in NDVI values of ≥ 0.25 to be indicative of healthy vegetation during their monitoring of the curing of grasslands in Australia. As such, further pre-processing, include image co-registration of pixels undertaken for both April and October periods where a base image, i.e., the latest image of 2018 is used to subset the remaining images. The purpose of co-registration is to correct all pixel shifts between different years to ensure pixel alignment and spatial consistency by snapping pixels according to the pixel placements in the base image. Finally, a threshold value of ≥ 0.25 is applied to NDVI satellite images in order to obtain binary vegetation cover images for all evaluated years for both months, i.e., April and October.

3.2. Area Change Analyses

After performing image co-registration, changes in vegetation area are obtained through direct comparison, e.g. the difference between binary images of NDVI data. Here, the changes in binary values demonstrate whether vegetation within a pixel and its base value has decreased, remained unchanged, or increased. Two different types of area change analyses are applied on the April and October datasets, respectively; (i) comparing vegetation status between base year (2003) and the subsequent 3-years intervals (i.e., 2006, 2009,... 2018) to measure the variation in vegetation over time relative to vegetation of the base year, and (ii), calculating the difference between every 3-year interval (e.g., 2006-2009) to quantify and isolate changes within shorter time frames (Section 4.1).

3.3. Trend Analysis

Trend analyses are carried out using the Mann-Kendall (MK) test, which represents a non-parametric test to statistically assess monotonic trends (positive, negative, or no trend) of a variable within a predetermined significance level over time (Vousoughi et al., 2013). The MK test does not require data to follow any specific probability distribution and is able to be completed under most circumstances as it is insensitive to outliers (e.g., extreme climate) or data gaps as long as the number is not too large, i.e., $\sim>40\%$ (Yadav et al., 2014).Also, since the input NDVI datasets of both April and October months for each year are independent observations with the respective time series for April or October from 2003 to 2018 having only 16 values, tests for autocorrelation and normality in each data series will not be very significant. For this investigation, the MK test is used to produce a Z-score map that displays linear trends (a single trend direction assumed), which are unique to each individual pixel for both April and October NDVI datasets from 2003 to 2018, respectively. A hotspot map is thereafter generated using the p-values obtained from MK test, respectively, for both NDVI datasets that identifies pixels that continuously experienced statistically significant decreasing trends for all the evaluated years, i.e., 2003 to 2018.

3.4. Anomaly Analysis

The purpose of an anomaly analysis is to detect the change of NDVI in the data by calculating the deviation from the overall mean (Andrew et al., 2017). In order to calculate anomalies for both areas' evaluated months, i.e., April and October, NDVI mean is calculated for the entire period (2003-2018) for April as well as October months. For our purpose, only NDVI values that are ≥ 0.25 are used and NDVI anomalies are calculated for each year by subtracting each pixel value from the overall mean. This process results in NDVI anomaly maps of each year from 2003 to 2018 for both April and October datasets, respectively. The status of vegetation cover expressed as anomalies maps with vegetation cover areas that are above the mean (increased), close to mean (no change), and below the mean (declined) in Section 4.2.1. Following this principle, the NDVI anomalies are calculated for each pixel using (Yang et al., 2014)

$$X_{Anomaly}(i,j) = X(i,j) - \frac{1}{n}\sum_{j=1}^{n} X(i,j), \tag{1}$$

where X represents the NDVI values, i is the month (e.g. April or October), j is the year, and n is the total number of years. In this case, two sets of NDVI anomalies are calculated for April and October months to obtain area of vegetation that have changed in regards to the overall mean. The Colorado Centre for Astrodynamics Research (CCAR) mascon visualization tool offers a 'deseason' option that presents the gridded Jet Propulsion Laboratory (JPL) GRACE total water storage (TWS) data as TWS anomalies, which signifies readily present TWS anomaly data that requires no further calculations and can be used with the calculated NDVI anomalies for further analyses, i.e., horspot areas evaluation.

3.5. Principal Component Analysis (PCA)

The principal component analysis (PCA) represents a statistical method that is able to reduce the dimensionality of BoM Australia-wide rainfall data but still retain the most dominant spatio-temporal variations of the original dataset (Awange et al., 2019, 2020). Here, PCA expresses the original dataset by modes each represented by, i.e., empirical orthogonal functions (EOFs) representing spatial patterns and principal components (PCs time series) representing temporal variabilities. In this study the number of modes required to adequately represent the dimensionality of the original dataset is selected so that the cumulative variance reflects at least 95% of the variability of the original dataset (Preisendorfer., 1988). While the original dataset can be recovered through the sum of all EOFs multiplied by their respective PCs, for a single PCA mode, the multiplication of the respective pair of EOF and PC represents the spatio-tempoiral variability contained by that mode. The study of the most dominant PCA modes can help in a better understanding of the relationship between rainfall and vegetation changes.

4. Results & Discussion

4.1. Temporal evolution of vegetation anomalies

4.1.1. Vegetation change of different year intervals from 2003

The vegetation area for both April and October datasets are derived for 2003, respectively, and are used as references (e.g., base year) for comparison with every three year's data up to 2018, i.e., 2003-2006, 2003-2009, 2003-2012, 2003-2015, and 2003-2018, as shown in Figure 2. For April, the highest total vegetation area decline is for the 2003-2006 period, with an overall 13.85% decline of the total vegetation areas during that period. According to Figures 2A, C, and E, areas of vegetation decline occur primarily within the northern, eastern, central and south-eastern parts of Australia. Furthermore, April in this period (2003-2006) has also experienced an increase of 14.71% of total vegetation areas. For October, the period 2003-2006 has an increase by 11.02% of total vegetation coverage, with areas of vegetation increase primarily being in the northern and western to central parts of Australia (Figures 2B, D and F), some of which are the same areas of vegetation increase during the month of April within the same period (Figure 2E). This possibly indicates a period of consistent growth within April and October during the period 2003-2006. As a general interpretation, the results indicate that the wet period had mostly impacted on Western Australia while little to no impact is noticeable in northern, central and eastern Australia, where vegetation is largely decreasing (Ma et al., 2016).

Vegetation cover in April appears to have experienced considerable decline by 12.11% over almost the entire Australia for the interval 2003-2009 in comparison to 2003. In October within the same period, the total areas of vegetation show a decrease of 8.32%, while the total area of vegetation for period 2003-2009 increased by 6.37%. This period (2003-2009) coincided with the Millennium Drought (Van Dijk et al., 2013), which may justify vegetation cover decline as the most prominent reason.

For the 2003-2012 period, the total area of vegetation increased significantly in the month of April as demonstrate by a highly positive deviation from the overall mean while during the same period, some areas experienced decline, i.e., negative deviation from the overall mean. Areas of vegetation cover increased by 24.26% compared to a decline of only 4.28%. This could indicate that the impact of the Millennium Drought was compensated by noticeable increase

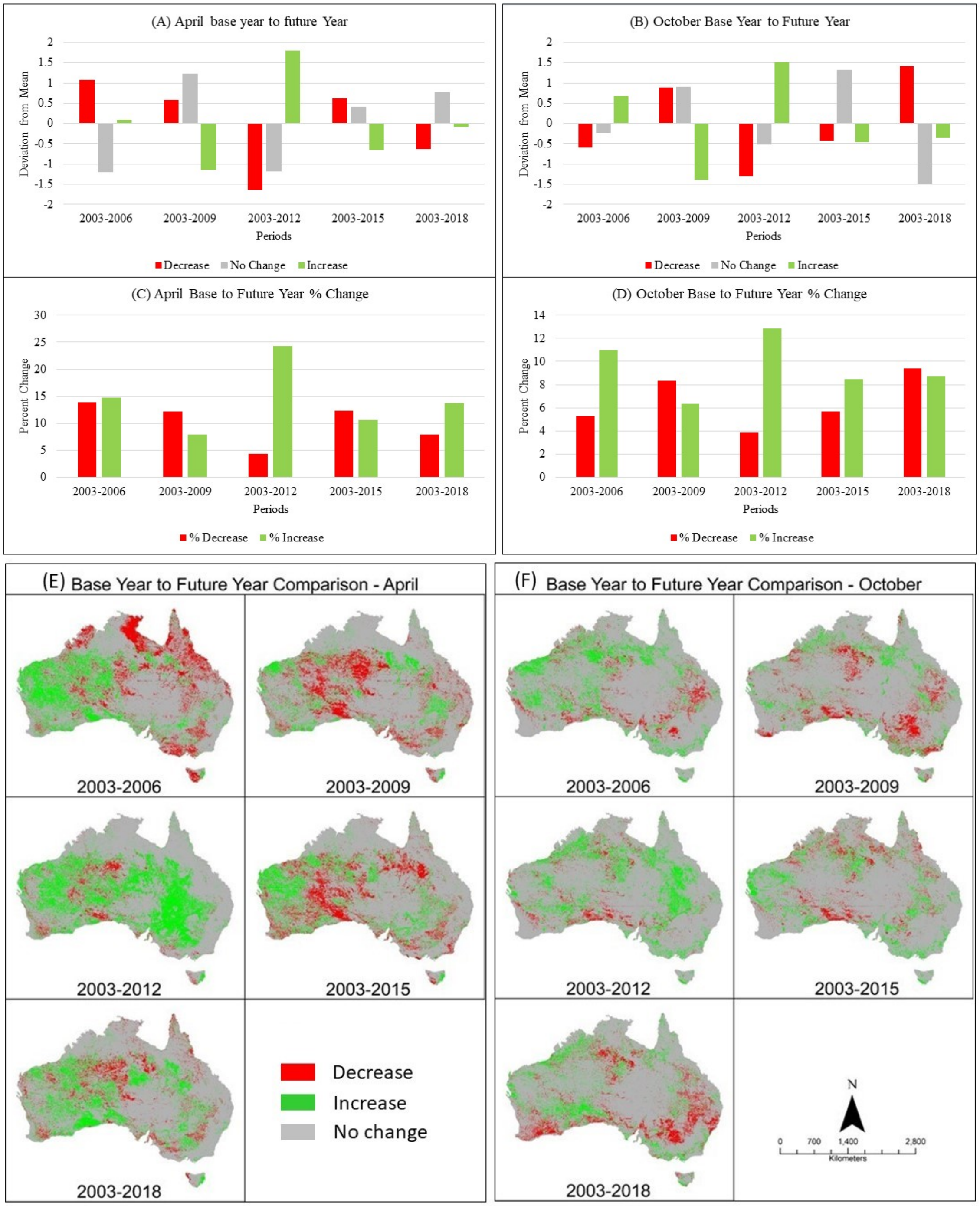

Figure 2: The Figure represents three-year changes in vegetation areas for April and October compared to 2003. Figures A, C, and E (left panels) represent April 2003 (Base year) compared to 2006, 2009, 2012, 2015, and 2018 (Future Years) while B, D, and F (right panels) represent October 2003 (Base year) compared to 2006, 2009, 2012, 2015, and 2018 (Future Years) for temporal vegetation change analyses.

in vegetation cover, e.g., between 2009-2012, where the net vegetation cover increase was much larger than the net decrease between 2003-2009. Similarly, areas of vegetation cover with increase in October is measured to be above the overall mean with an increase by 12.86% of the total vegetation coverage. Meanwhile, the areas of vegetation cover decreased by 3.88%, which is below the overall mean. This indicates a period of vegetation increase for both April and October for the 2003-2012 period, and in particular, a significant increase can be observed over the Murray-Darling Basin (Figures 2E and F) as a result of 2011-2012 floods. The occurrence of vegetation increase can be explained by a strong La Niña event in early 2010 that brought high precipitation that affected mainly areas within eastern Australia, which signified the end of the Millennium Drought (King et al., 2014; Ma et al., 2015; Van Dijk et al., 2013). The strong La Niña event can be observed from the Principal Component Analysis (i.e., PC1 and PC2; Figure 7 in Section 4.2.4), which shows a large positive deviation that indicates above average rainfall in eastern Australia (strongly along the east coast) in the 2010-2011 period, and below average rainfall for other parts, i.e., central, southern and Western Australia in early 2010. This is followed by another positive deviation at the end of 2010 that is reflected by a significant increase of total water storage as displayed in Figure 6 that recorded a maximum in December 2010.

The 2003-2015 April period shows larger areas of vegetation cover decrease in comparison to other periods, i.e., 2003-2012, with a total of 12.25% compared to areas of vegetation cover that increased by 10.63% for same month. For October, areas of vegetation cover declined by 5.65%, which is lower than the total area of vegetation cover that experienced an increase of 8.44%. Areas of increased vegetation cover largely reduced from 24.26% to 10.63% for the month of April between the periods of 2003-2012 and 2003-2015. The reduction of vegetation areas after April 2012 corroborates the findings of Ma et al. (2016) that recorded a transition towards drier conditions after the 2010-2011 wet period, which reduced the availability of water vital for vegetation growth. Effectively, the positive impact from the strong La Niña event lasted only for 1-2 years, e.g., may be interpreted as a short wet-period within the Millennium Drought that seemed to have lasted beyond 2012 (King et al., 2014; Ma et al., 2015; Van Dijk et al., 2013).

Finally, for the 2003-2018 period, which represents a long-term period when compared with other periods, i.e., 16 years of temporal vegetation changes, for the month of April, areas of vegetation cover a larger overall increase than decline. This behavior is quantified by the percentage change in which overall areas of vegetation increased by 13.77% throughout the study period compared to a decrease of 7.82%, indicating that overall, Australia experienced an increase in vegetation cover for the month of April over the 2003-2018 period. For the month of October, areas of vegetation cover decreased by 9.41%, i.e., slightly larger than areas of vegetation cover increase of 8.71%, signifying that vegetation cover slightly decreased within the study period of 2003-2018.

4.1.2. Vegetation change between 3-year interval epochs

Vegetation area changes for each 3-year interval within the period 2003-2118, i.e., 2003-2006, 2006-2009, 2009-2012, 2012-2015, and 2015-2018, are calculated for both April and October datasets, respectively. Area change analysis between epochs enables vegetation activities to be measured during a specific 3-year period. As mentioned in section 4.1.1 in regards to 2003-2006 period during April, total area of vegetation cover decreased by 13.85%, while the areas of vegetation cover increased by 14.71% during the same period (Figure 3C). As already identified in section 4.1.1, areas of vegetation decline during this period occur primarily within the northern, eastern, central and south-eastern parts of Australia (Figure 3E). Within the same epoch, most areas that showed a decrease in vegetation cover in April are showing no change in October along with some other areas experiencing vegetation increase (Figure 3), indicating that these areas experience continued vegetation decrease during this period.

Changes in April during the 2006-2009 epoch generally show an opposite behavior to the changes during the 2003-2006 epoch (Figures 2E and 3E). Areas that previously showed a decrease/increase now show an increase/decrease, e.g., indicating that vegetation area loss/gain during 2003-2006 has been reversed during 2006-2009. Areas of vegetation declined in April by 16.83%, while areas of vegetation cover increased by 11.74%. Vegetation in October visualized in Figure 3F also displays an inverse behaviour in which previous areas of vegetation increase in 2003-2006 are transformed to areas of vegetation decrease and vice versa during 2006-2009. For October, the 2006-2009 epoch measured 11.51% of overall vegetation decline in comparison to areas of vegetation increase by 3.84% (Figures 3B and D). The vegetation cover areas status between April and October indicate that the decrease of vegetation is more prominent within 2006-2009 compared to 2003-2006 period, which experienced a wet period during 2005-2006 (Ma et al., 2016).

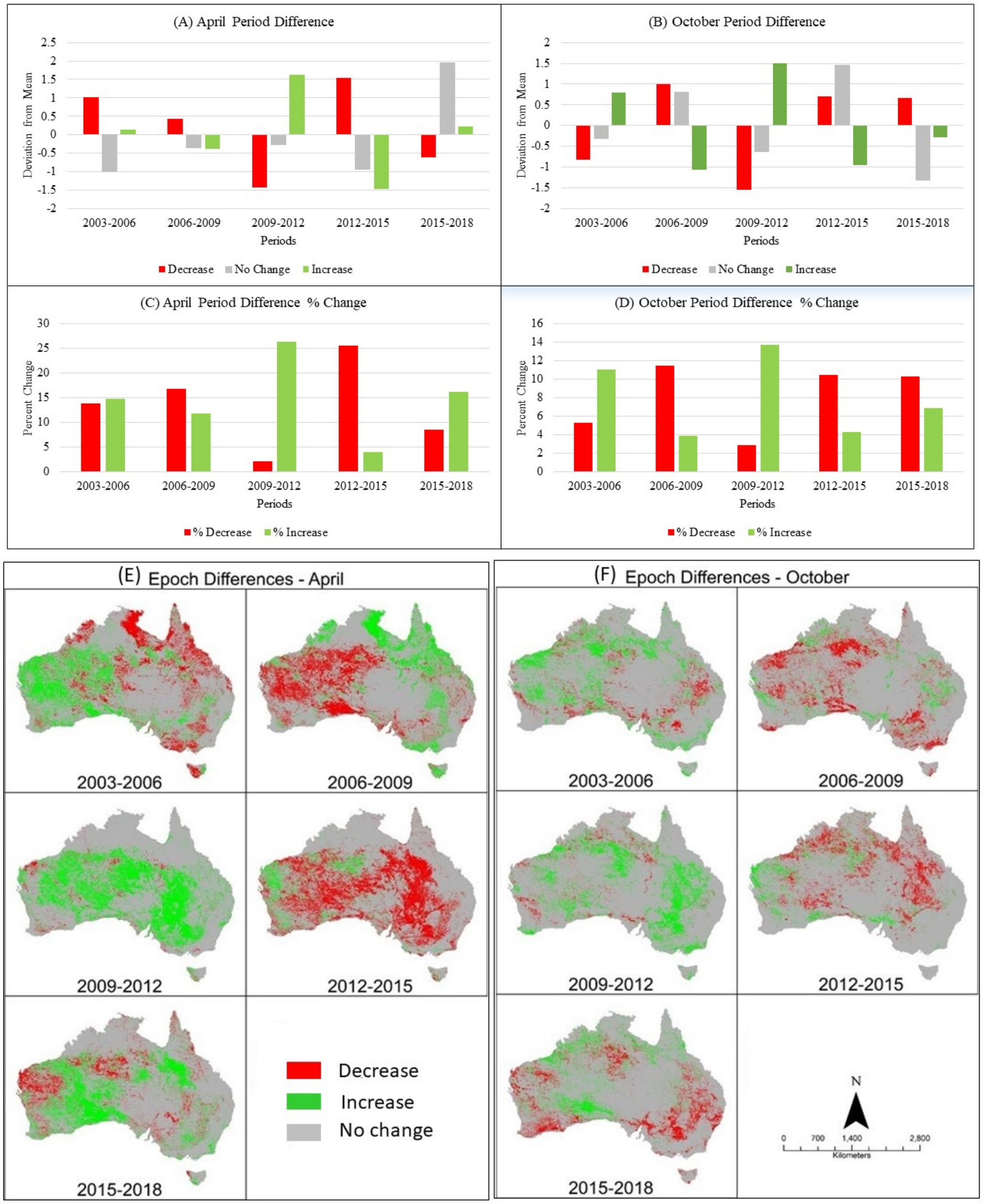

Figure 3: Figures A, C, and E represent April Epochs, i.e., 2003-2006, 2006-2009, 2009-2012, 2012-2015, 2015-2018, and B, D, and F represent October Epochs, i.e., 2003-2006, 2006-2009, 2009-2012, 2012-2015, 2015-2018 for temporal analysis for vegetation variation.

The 2009-2012 epoch displayed considerable increase in the area of vegetation coverage across Australia for the month of April (Figures 3C and E), with a total area increase of 26.37% and loss of vegetated areas of only 2.11%. During the month of October, however, areas of increased vegetation that have in April reduced from 26.37% to 13.76%, while vegetation areas decreased in October, remained at 2.83% (i.e., a similar low level as in April). The growth of vegetation over eastern Australia shown in Figure 3F remained as areas of increase vegetation as observed in April. The high increase of vegetation areas can be attributed to a strong La Niña event that resulted in high amounts of rainfall greatly affecting the eastern Australia (King et al., 2014; Ma et al., 2015; Van Dijk et al., 2013), which can also be seen in Figure 7 during 2010-2011 as previously explained. Vegetation increase during this epoch (2009-2012) corroborates the results of Ma et al. (2015), which reported Australia as being one of the strongest global land carbon sinks in 2011.

Vegetation cover areas that increased during 2009-2012 do not appear to be present within the 2012-2015 epoch as areas of declined vegetation can be observed in Figures 3A and 3B to have encompassed most of the areas of vegetation increase that were present during 2009-2012 epoch. For April, areas of decreased vegetation were 25.58% of total vegetation area in 2012-2015 compared to the 2009-2012 epoch, which recorded areas of decreased vegetation to be 2.11%. Areas of increased vegetation before suffered a large reduction from 26.33% in 2009-2012 to 3.98% in 2012-2015. Vegetation area recorded for the month of October in 2012-2015 also follow a similar pattern to that of April in which vegetation showed opposite behaviour to what was recorded in 2009-2012, in which areas of vegetation that decreased before in 2009-2012 period rose from 2.83% to 10.49%, while previously areas of increased vegetation now reduced from 13.76% to 4.3%. Vegetation decrease and increase show inverse pattern between the 2009-2012 and 2012-2015 epochs for both April and October, which can be explained by a transition from anomalously high rainfall in 2010-2011 to drought conditions in 2012 that exacerbate dry conditions detrimental for vegetation growth (Ma et al., 2015).

The final epoch of 2015-2018 experienced an increase in vegetation areas of 16.13% whereas areas of vegetation reduced by 8.58%, indicating that the 2015-2018 epoch represents a period of climatic conditions favouring vegetation growth for the month of April. These multi-year variations are demonstrated in Figure 3E in which various areas that suffered vegetation decrease during the previous 2012-2015 epoch now transitioned towards areas of vegetation increase. In the month of October, areas of vegetation that declined remained higher than areas of vegetation that increased, i.e., 10.33% and 6.85%, respectively. Areas of decreases vegetation in October did not experience large changes, i.e., 10.49% in 2012-2015 and 10.33% in 2015-2018, while areas of increased vegetation experienced a growth from 4.3% to 6.85%. The overall vegetation area changes for the epochs in the month of April show areas of vegetation that decreased before are further declining, indicating that the decreases in vegetation areas are lessening whereas the overall trend of areas of vegetation that decreased for the epochs in October suggests otherwise, in which the trend for areas of vegetation cover decrease is rising.

4.2. Evaluation of hotspot areas

4.2.1. Mann-Kendall Trend Analysis for MODIS NDVI Anomalies

The Mann-Kendall trend analysis detects linear trend of pixel behaviour, taking into account whether there have been more occurrences of NDVI anomaly below the mean versus above the mean and vice versa. In order to evaluate pixel values during a specific year, maps that represent anomalous NDVI values of every year between 2003-2018 are generated for both April and October NDVI datasets (Figures 4A and B). These figures show the temporal variation for NDVI anomalies values for both months covering every consecutive year from 2003 to 2018. Examining these figures, they often show a north-south pattern that relates to the north-south rainfall seasonality (see also PCA analysis of rainfall in Section 4.2.4). For example, April maps show that northern regions experienced some areas with NDVI values below average. This is most likely related to below average rainfall as the rainy season ends in April for the northern region except 2011 (flood events). The same pattern is observed for southern regions in the October which coincides with the end of rainy season.

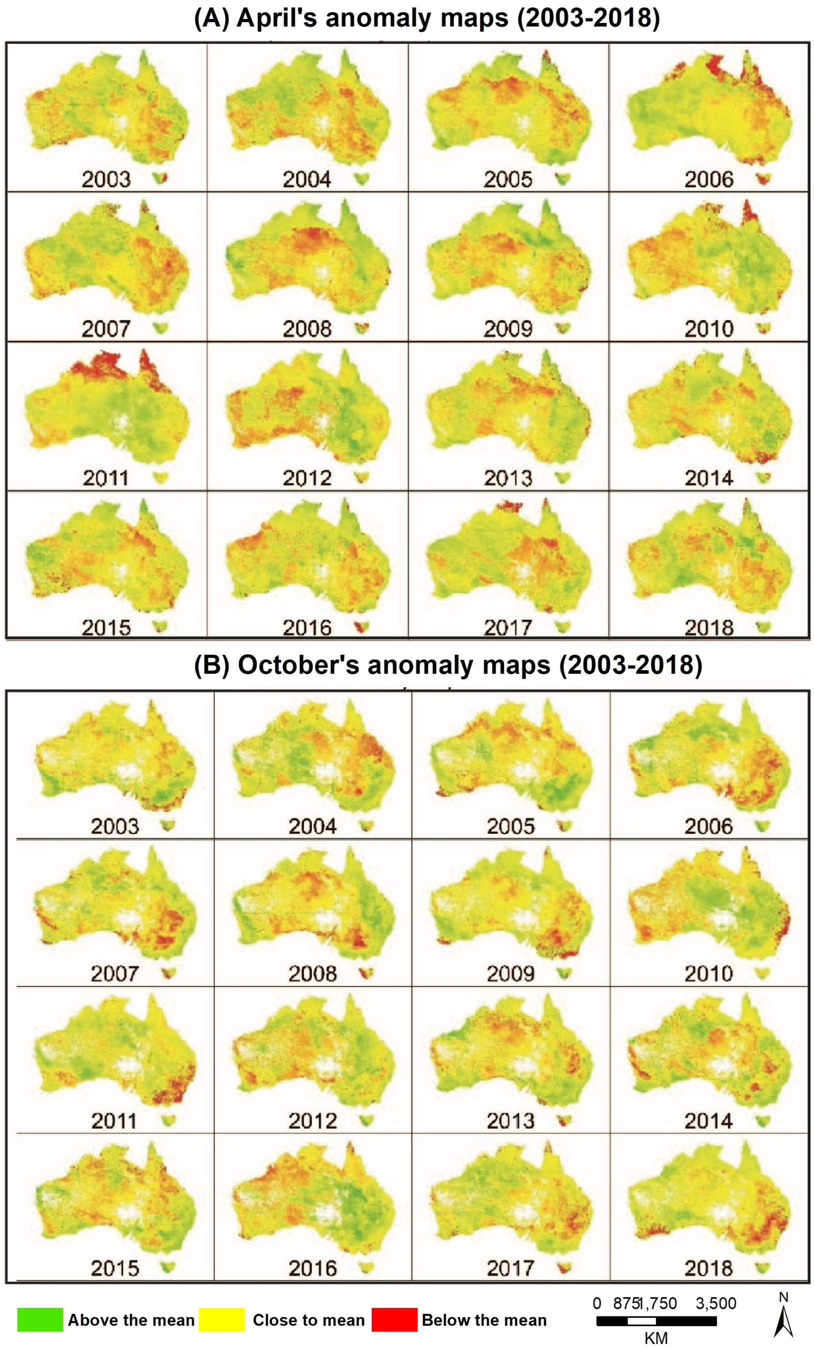

Figure 4: Anomaly maps for (a) April and (b) October, for 2003-2018 period. NDVI values smaller/larger than mean for each year are shown as red/green while yellow represents NDVI values that are close to the long-term mean (regarded as similar to mean).

4.2.2. Identification of hotspot areas

Figure 5 presents the results of the Mann-Kendall trend analysis of all individual pixels with a p-value < 0.05 for both the month of April and October, respectively. Each pixel is represented by its own unique linear trend classified as either to be an increase in vegetation, no change in vegetation, or a decrease in vegetation. Figure 5A displays vegetation changes for the month of April during the period (2003-2018), where vegetation is shown to be increasing in the south-west and south-east areas. Figure 5B shows the vegetation status for the month of October and how it has behaved over every year within the study period in which there are discernible areas of vegetation decrease that can be identified unlike the month of April in Figure 5A. Within Figure 5B, pixels that display negative trends of vegetation growth can be visualized to be situated along the coastline of South Australia, and mid to south of Western Australia.

Areas with decreasing trend in October are highlighted and labelled A2 and B2 in Figure 5B. The same areas are also identified in Figure 5A (labeled A1 and B1) for the month of April for the purpose of comparison of vegetation behaviour in the identified areas between April and October. Area A2 (hotspot regions that have constantly experienced statistically significant decrease in NDVI) in Figure 5B and area A1 in Figure 5A display pixels located within south Western Australia in which vegetation in October indicated by area A2 is largely recorded to have a decreasing trend in the middle while increasing along the east and south-east. Area A1 for the month of April display some increase in the north, east, and south-east (within the highlighted area), while experiencing no change in the middle. For both area A1 and A2 within the highlighted area, pixels along the east and south-east of the highlighted area boundary show a trend of vegetation increase for both April and October throughout the study period. Within the middle of the highlighted area boundary, area A2 displays pixels with a trend of vegetation decrease whereas area A1 displays largely no change, indicating a lack of vegetation growth in that area for April and October over the study period.

Area B2 (hotspot regions that have constantly experienced statistically significant decrease in NDVI) labelled in Figure 5B represent pixels along the coastline of South Australia in October and is comparable to area labelled B1 in Figure 5A for the month of April. Pixels within area B2 measured a trend of vegetation decrease along the South Australian coastline whereas area B1 shows no change, signifying that the pixels have not experienced vegetation growth for either months.

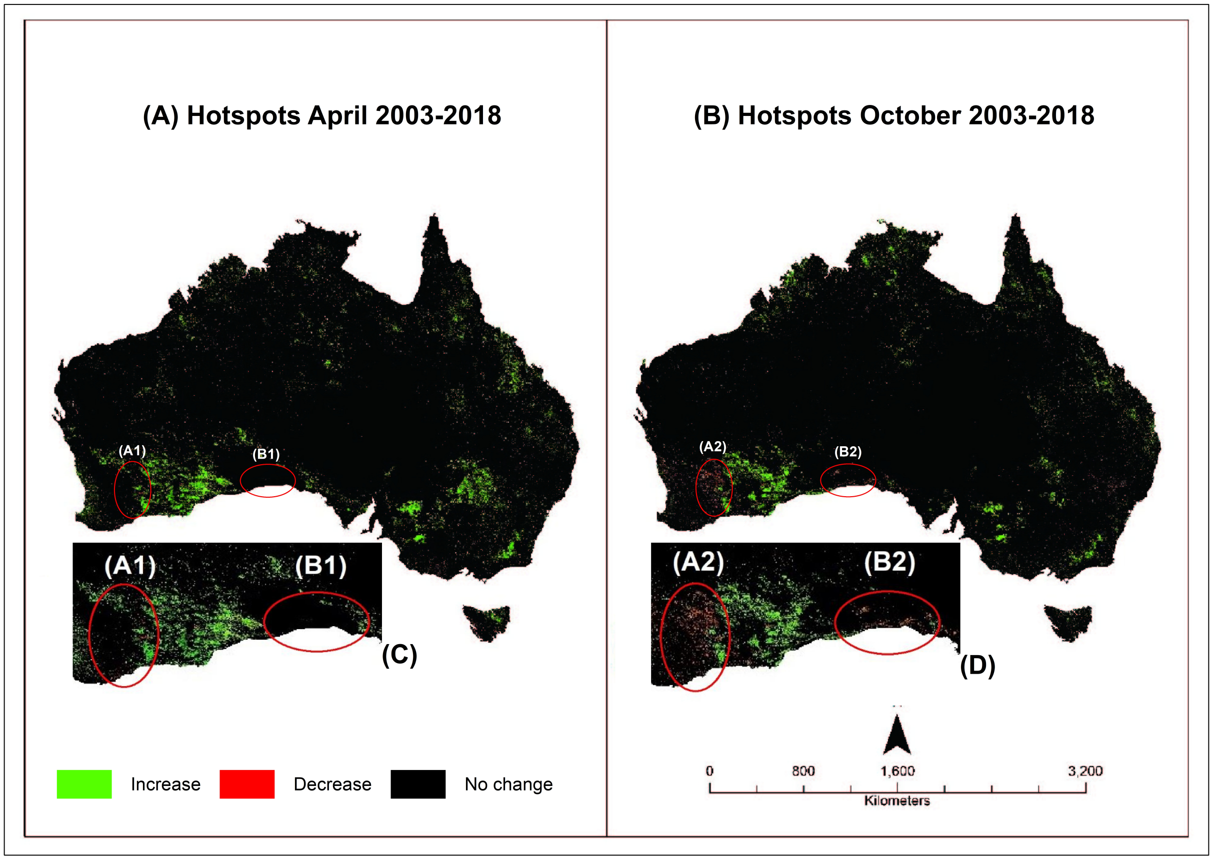

Figure 5: Results of the Mann-Kendall trend analysis, (A) April vegetation with A1 and B1 representing areas in the month of April that correspond with identified hotspots for Western Australia and South Australia, respectively, and (B), October vegetation and hotspots identified, i.e., A2 and B2, in the month of October 2003-2018 for same locations. Only pixels with p-values < 0.05 are shown for both months, i.e., April and October. The black color indicate non-significant trends of vegetation. (c) and (D) are zoomed hotspot inset maps for April and October, respectively.

4.2.3. Hotspot evaluation with corresponding GRACE Mascon Data

Soil moisture represents an important hydrological component towards vegetation growth as it is where the vegetation root zone lies (Agutu et al., 2017; Khaki et al., 2019). Previous studies have discovered a strong positive relationship between soil moisture and NDVI across mainland Australia when soil moisture precedes NDVI by one month (Chen et al., 2014; Yang et al., 2014). It should be noted that this was a general assessment of soil moisture and NDVI, as soil moisture may vary regionally and locally across Australia. GRACE TWSA data derived from the mascon visualization tool represents the sum of surface water, groundwater, soil moisture, vegetation water, ice and snow (Awange et al., 2011; Jiang et al., 2014). For reasons explained in Section 2.3, GRACE TWSA data is used to represent the soil moisture changes throughout the study period and compared here through visualization to assess relative changes between vegetation and soil moisture within the selected hotspot areas (Section 4.2.2). Changes in soil moisture are assumed to be dominant as within the hotspots, surface water changes are negligible in terms of impacts on vegetation growth and so are groundwater changes. The hotspot areas experience no snow nor ice and as such, changes associated with them do not exist.

Figure 6 shows relative hydrological changes for the two hotspot areas, i.e., A1/A2 and B1/B2, throughout the study period. As mentioned earlier, the Millennium drought had adverse effects on Australia-wide vegetation from 2001-2009 (Ma et al., 2016). The effects of this can be observed in Figures 6A and 6B from 2003-2010, in which the TWSA of both mascons display a decreasing trend. GRACE TWSA in Figure 6B is shown to experience a decreasing trend of larger magnitude during this period compared to Figure 6A, which may be due to the fact that area B1/B2 lies closer to the coast than area A1/A2, as being situated near the coastline may have seepage effects from the ocean (see e.g., Awange et al. (2009)).

As mentioned earlier in Section 4.1.2, vegetation increase was observed in both April and October during the epoch 2009-2012, which can be explained by a strong La Niña event in 2010-2011 that brought high precipitation that affected mainly areas within eastern Australia (King et al., 2014; Ma et al., 2015; Van Dijk et al., 2013). Although the La Niña event affected eastern Australia greatly, mascon TWSA illustrate large increase between December 2010 - February 2011 in both hotspot areas that are located within south Western Australia and along the coastline of South Australia, respectively. The Indian Ocean Dipole (IOD) has been found to affect rainfall patterns of western and southern Australia during the winter and spring (King et al., 2014). The steep and large increase of the mascon TWSA during December 2010 - February 2011 could possibly be due to a negative IOD event that co-evolved with the La Niña conditions in 2010 (Forootan et al., 2016), bringing high precipitation towards the hotspot areas that may have recharged the TWS of the areas. The steep increase in TWSA within both hotspot areas were not long lasting as TWSA can be observed to experience a large reduction after 2012. This may be due to a transition towards anomalously dry conditions recorded in 2012-2013 (Ma et al., 2015). After 2013, TWSA for both areas can be observed to exhibit stabilizing behavior (e.g., no significant increase or decrease) for the remainder of the study period.

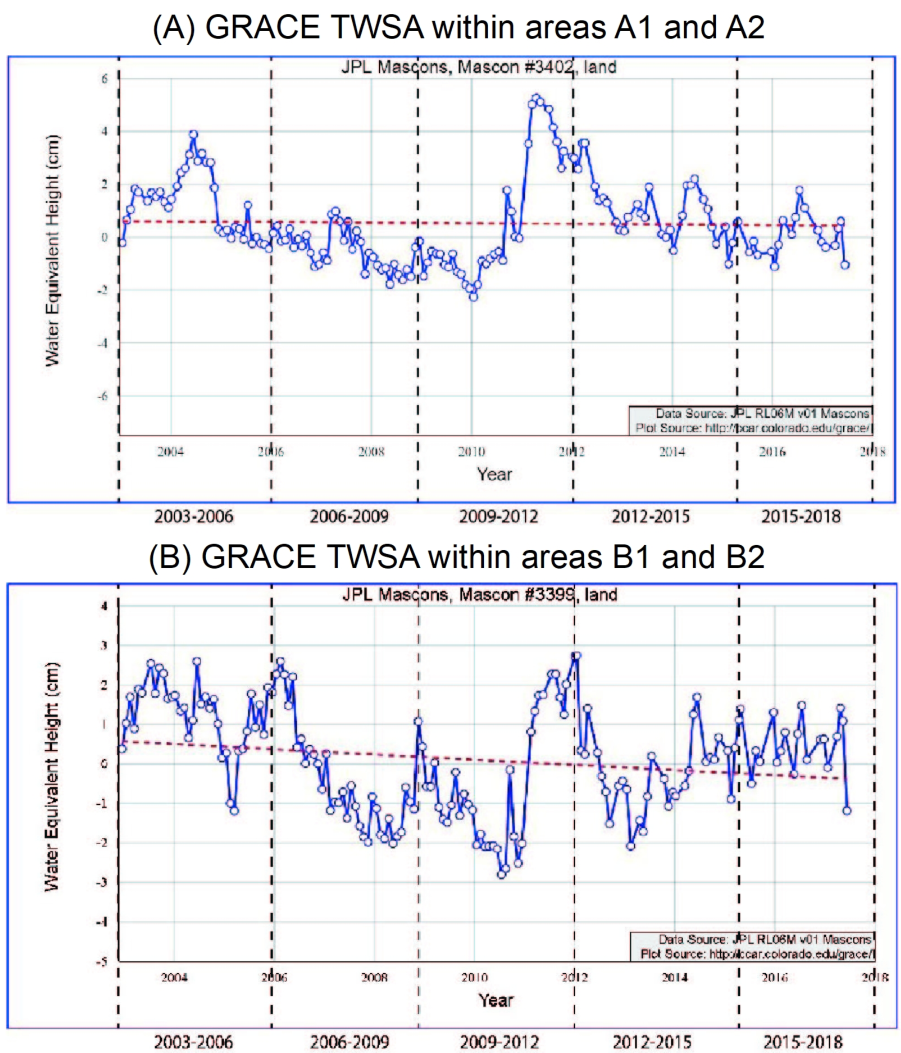

Figure 6: GRACE TWSA hydrological changes over the hotspot areas from 2003-2018. Dividers of epochs at every 3-year interval are also illustrated.

4.2.4. Principal Component Analysis (PCA) evaluation of BoM rainfall data over hotspots

Results of the PCA calculations on monthly BoM rainfall data are displayed in Figure 7, which consist of the three most dominant PCA ranked from higher to lower variance; total variance accounts for more than 99% of the total variance) that collectively represent the total Australia-wide rainfall from 2003-2018. PC1 shows variation of annual rainfall pattern that accounts for 84.3% of the total rainfall variance, PC2 and PC3 represent anomalous extreme climate events accounting, respectively, 9.0% and 6.6% of the total variance. In terms of PC1, rainfall exhibits regular annual variation across Australia throughout the study period, in which rainfall for north and northeast of Australia occurs mostly during the summer whereas rainfall south and southwest occurs during the winter (see also Awange et al. (2009, 2011); Rieser et al. (2010)).

Rainfall variability are more distinguishable within PC2 and PC3. During the millennium drought that coincide within 2003-2009 period of the study, PC2's time series shows increasingly positive values that, together with the corresponding EOF, indicate an increasing lack of rainfall for both hotspot areas A and B. This corroborates with Figure 6A and B that displays negative TWSA trends during 2003-2009 for both hotspots, which may be due to the lack of rainfall within the hotspot areas, i.e., A1/A2, and B1/B2 in Figure 7. Rainfall anomalies of the PC3 time series also illustrate similar behaviour during 2003-2009, in which the driest event occurred in 2008. The impact on vegetation of the extreme dry conditions in 2008 resulted in a decrease of vegetation that can be observed in Figures 3E and 3F during the 2006-2009 epoch for both April and October, respectively.

Both hotspots' TWSA in Figure 6A and B showed a steep and large positive trend between December 2010 - February 2011. The hydrological changes of TWSA can be explained by rainfall anomalies as illustrated in the time series of PC1 and PC3, by which a considerable increase in rainfall can be observed to have occurred within both hotspot areas towards the end of 2010 and the beginning of 2011. The impact of the precipitation event on NDVI anomalies is displayed within Figures 4A and B, whereby both April and October 2011 anomalies map showed signs of greening within the hotspots.

However, the greening event was short-lived, as anomalously dry conditions became again more pervasive after 2012 (Ma et al., 2016). The decline in rainfall is predominantly seen PC1 showing considerably reduced rainfall during the summers 2011-12, 2012-13 and 2015-2016. To a much lesser extent this can be seen in PC3. Vegetation after 2012 is shown to be decreasing Australia-wide, particularly for the eastern states as outlined in Figures 3E and 3F in 2012-2015 for both April and October, respectively. In general, rainfall variability over hotspot A1/A2 during 2012-2015 is shown to be decreasing whereas rainfall variability over hotspot B1/B2, although low, does exhibit positive rainfall anomalies but may not be enough to sustain vegetation increase due to possible runoff and evapotranspiration or anthropogenic activities.

In summary, changes in both hotspots relative to hydrological changes based on GRACE TWSA reflect a similar decreasing trend from 2003-2009, which can be attributed to the millennium drought that occurred within this period. For the same period, rainfall as shown in the PCA results illustrate negative anomalies for both hotspots in Western Australia and in South Australia, thus contributing towards the low level in TWSA as a lack of rainfall may prevent water storage recharge. Mascon TWSA is shown to exhibit an increasing trend in 2009-2012 that peaked in 2011. This increase is likely due to a negative IOD event that co-evolved with La Niña conditions in 2010-2011, causing high precipitation towards the hotspot areas. This increased precipitation event is evident in the PC1 and PC3 time series as an increase in rainfall can be observed to have occurred within both hotspot areas towards the end of 2010 and the beginning of 2011. Both mascon TWSA then exhibit a steep negative trend after 2012, which may be due to a transition towards dry conditions recorded in 2012-2013. Rainfall within 2012-2015 differs for both hotspots as rainfall anomalies over hotspot A1/A2 (in Western Australia) are found to indicate below average rainfall and over hotspot B1/B2 to show above average rainfall. However, vegetation after 2012 is found to be decreasing Australia-wide, indicating that the positive anomalies of rainfall over hotspot B1/B2 (in South Australia) may not have sustained the total water storage of that area due to possible runoff and evapotranspiration or anthropogenic activities. The decrease in TWSA seemed to have stopped after 2012 indicating some stabilizing behavior for the remainder of the study period.

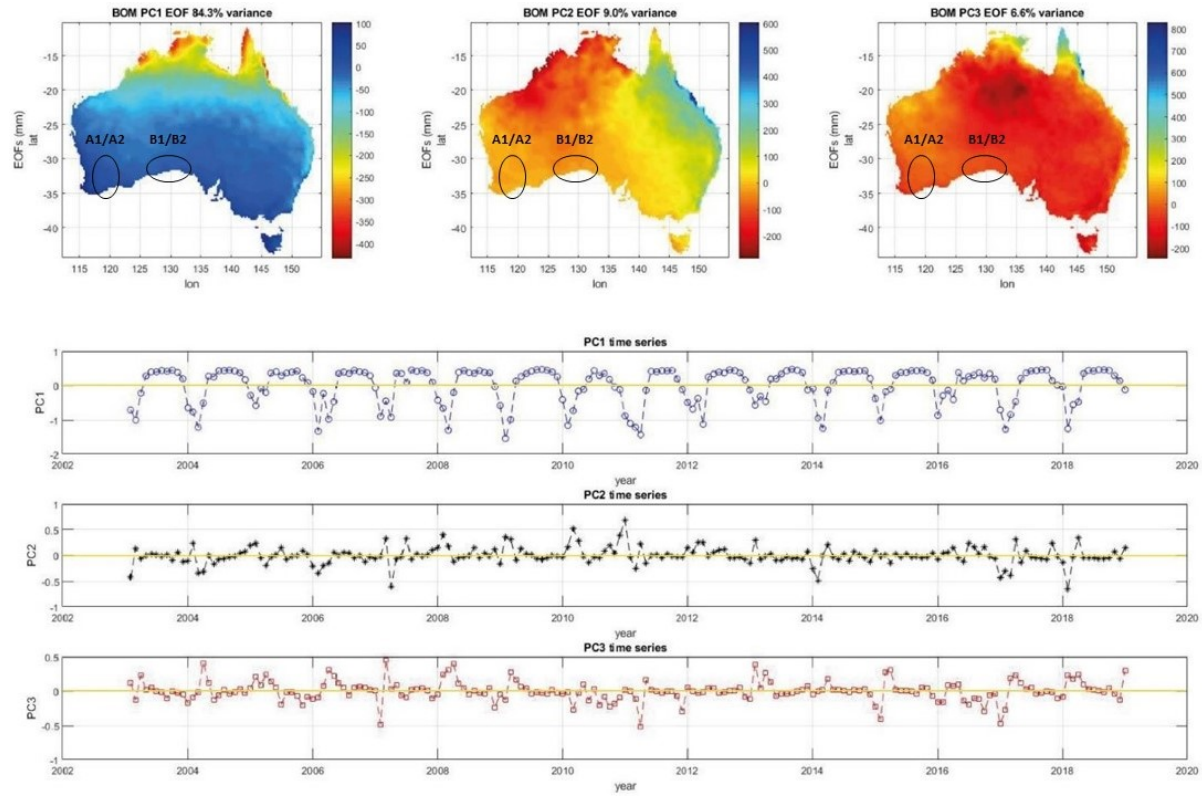

Figure 7: Spatial Pattern and time series of the first three most dominant PCA modes of Australia-wide rainfall 2003-2018. PC1 indicates the annual rainfall variability while PC2 and PC3 capture some extreme climatic events. A1 and B1 represent areas in the month of April that correspond with identified hotspot areas A2 and B2 in the month of October for Western Australia and South Australia, respectively.

5. Conclusion

This study employed MODIS data at its native spatial resolution ($0.002413° \times 0.002413°$) rarely used before to investigate the effects of extreme climate on Australia's green cover during 2003-2018 for the months of April and October with the aim of determining the state of vegetation and its changes. Also, the identification of the NDVI change "hotspots", and relating these changes to GRACE total water storage changes and Australia-wide rainfall have not been previously undertaken. This study found that Australia's vegetation cover experienced considerable temporal variation throughout the study period 2003-2018. In particular:

1. Both April and October show the same vegetation increasing pattern when the rainy season ended in northern and southern regions, respectively. In April, the vegetation exhibited more increase in northern Australia and more decrease in south while for October, it experienced more decrease in north and more increase in south throughout 2003-2018 period.
2. Analysing 3-year interval changes during the period 2003-2018 indicated that for April, vegetation decrease was very high for the 2006-2009 and 2012-2015 periods while 2009-2012 and 2015-2018 showed increase in vegetation. Within these epochs, October shows similar behaviour with the exception of the 2015-2018 period, in which vegetation decrease was shown to be higher. The variation in rainfall (wet and dry seasons) during the evaluated years might explain the increase and decrease in vegetation cover changes for Australia-wide indicating some multi-year variation.
3. Two hotspot regions that constantly experienced statistically significant decrease in NDVI are identified in Western Australia and South Australia, where vegetation decrease is noticed in October and no change in April during 2003-2018.
4. Both hotspots above experienced hydrological decrease and increase based on GRACE TWSA for the periods 2003-2009 and 2009-2012, respectively. These hydrological variations for both hotspot areas might be attributed to the millennium drought for the 2003-2009 period and a negative IOD event that co-evolved with La Niña conditions leading to increased rainfall in 2010-2011 for 2009-2012 period.

6. Acknowledgment

Ashty Saleem is grateful for the opportunity offered to him by Curtin University, School of Earth and Planetary Sciences to undertake his postdoctoral studies. Joseph L. Awange would like to thank the financial support of the Alexander von Humboldt (AvH) Foundation that supported his time at Karlsruhe Institute of Technology in July-September 2019. He is grateful to the good working atmosphere provided by his hosts Prof and Hansjörg Kutterer and Prof Bernhard Heck.

7. References

References

Agutu, N. O., Awange, J. L., Zerihun, A., Ndehedehe, C. E., Kuhn, M., & Fukuda, Y. (2017). Assessing multi-satellite remote sensing, reanalysis, and land surface models' products in characterizing agricultural drought in East Africa. Remote sensing of environment, 194, 287-302, doi:10.1016/j.rse.2017.03.041.

Andrew, R. L., Guan, H., & Batelaan, O. (2017). Large-scale vegetation responses to terrestrial moisture storage changes. Hydrology and Earth System Sciences, 21, 4469-4478, doi:10.5194/hess-21-4469-2017.

Awange JL, Palancz B and V¨ölgyesi L (2020) Hybrid Imaging and Visualization. Employing Machine Learning with Mathematica - Python. Springer Nature International, Berlin.

Awange, J. L., Fleming, K. M., Kuhn, M., Featherstone, W. E., Heck, B., & Anjasmara, I. (2011). On the suitability of the 4×4 GRACE mascon solutions for remote sensing Australian hydrology. Remote Sensing of Environment, 115(3), 864-875, doi:10.1016/j.rse.2010.11.014.

Awange, J., K. Hu, & M. Khaki (2019), The newly merged satellite remotely sensed, gauge and reanalysis-based Multi-Source Weighted-Ensemble Precipitation: Evaluation over Australia and Africa (1981-2016). Science of The Total Environment, 670, 448-465, doi:10.1016/j.scitotenv.2019.03.148.

Awange, J. L., Schumacher, M., Forootan, E., & Heck, B. (2016). Exploring hydro-meteorological drought patterns over the Greater Horn of Africa (1979–2014) using remote sensing and reanalysis products. Advances in Water Resources, 94, 45-59, doi:10.1016/j.advwatres.2016.04.005.

Awange, J. L., Sharifi, M. A., Baur, O., Keller, W., Featherstone, W. E., & Kuhn, M. (2009). GRACE hydrological monitoring of Australia: Current limitations and future prospects. Journal of Spatial Science, 54(1), 23-36, doi:10.1080/14498596.2009.9635164.

Broich, M., Huete, A., Tulbure, M. G., Ma, X., Xin, Q., Paget, M., & Held, A. (2014). Land surface phenological response to decadal climate variability across Australia using satellite remote sensing. Biogeosciences, doi:10.5194/bg-11-5181-2014.

Chen, T., De Jeu, R. A. M., Liu, Y. Y., Van der Werf, G. R., & Dolman, A. J. (2014). Using satellite based soil moisture to quantify the water driven variability in NDVI: A case study over mainland Australia. Remote Sensing of Environment, 140, 330-338, doi:10.1016/j.rse.2013.08.022.

Chen, X., Wang, D., Chen, J., Wang, C., & Shen, M. (2018). The mixed pixel effect in land surface phenology: A simulation study. Remote Sensing of Environment, 211, 338-344, doi:10.1016/j.rse.2017.01.001.

Chen, Y., & Gillieson, D. (2009). Evaluation of Landsat TM vegetation indices for estimating vegetation cover on semi-arid rangelands: a case study from Australia. Canadian Journal of Remote Sensing, 35(5), 435-446, doi:10.5589/m09-037.

Donohue, R. J., McVICAR, T. R., & Roderick, M. L. (2009). Climate-related trends in Australian vegetation cover as inferred from satellite observations, 1981–2006. Global Change Biology, 15(4), 1025-1039, doi:10.1111/j.1365-2486.2008.01746.x.

Fleming, K., & Awange, J. (2013). Comparing the version 7 TRMM 3B43 monthly precipitation product with the TRMM 3B43 version 6/6A and Bureau of Meteorology datasets for Australia. Australian Meteorological and Oceanographic Journal, 63, 421-426.

Fleming, K., Awange, J., Kuhn, M., & Featherstone, W. (2010). Satellite Observations for Identifying Continental-Scale Climate Change over Australia. Nova Acta Leopoldina, 348, 1-9.

Forootan, E., Awange, J. L., Schumacher, M., Anyah, R. O., Van Dijk, A., & Kusche, J. (2016). Quantifying the impacts of ENSO and IOD on rain gauge and remotely sensed precipitation products over Australia. Remote sensing of Environment, 172, 50-66.

Hu, K. X., Awange, J. L., Kuhn, M., & Saleem, A. (2019). Spatio-temporal groundwater variations associated with climatic and anthropogenic impacts in South-West Western Australia. Science of The Total Environment, 696, 133599.

Huete, A., Didan, K., van Leeuwen, W., Miura, T., & Glenn, E. (2010). MODIS vegetation indices. In Land remote sensing and global environmental change (pp. 579-602). Springer, New York, NY.

Hughes, L. (2011). Climate change and Australia: key vulnerable regions. Regional Environmental Change, 11(1), 189-195, doi:10.1007/s10113-010-0158-9.

Jiang, D., Wang, J., Huang, Y., Zhou, K., Ding, X., & Fu, J. (2014). The review of GRACE data applications in terrestrial hydrology monitoring. Advances in Meteorology, 2014, doi:10.1155/2014/725131.

Jiao, T., Williams, C. A., Rogan, J., De Kauwe, M. G., & Medlyn, B. E. (2020). Drought impacts on australian vegetation during the millennium drought measured with multi-source spaceborne remote sensing. Journal of Geophysical Research: Biogeosciences, 125(2), e2019JG005145.

Khaki, M., Zerihun, A., Awange, J., & Dewan, A. (2019). Integrating satellite soil-moisture estimates and hydrological model products over Australia. Australian Journal of Earth Sciences, 1-13, doi:10.1080/08120099.2019.1620855.

King, A. D., Klingaman, N. P., Alexander, L. V., Donat, M. G., Jourdain, N. C., & Maher, P. (2014). Extreme rainfall variability in Australia: patterns, drivers, and predictability. Journal of climate, 27(15), 6035-6050, doi:10.1175/JCLI-D-13-00715.1.

Lewis, S. L., Brando, P. M., Phillips, O. L., van der Heijden, G. M., & Nepstad, D. (2011). The 2010 amazon drought. Science, 331(6017), 554-554, doi:10.1126/science.1200807.

Lu, H., Raupach, M. R., McVicar, T. R., & Barrett, D. J. (2003). Decomposition of vegetation cover into woody and herbaceous components using AVHRR NDVI time series. Remote Sensing of Environment, 86(1), 1-18, doi:10.1016/S0034-4257(03)00054-3.

Ma, X., Huete, A., Moran, S., Ponce-Campos, G., & Eamus, D. (2015). Abrupt shifts in phenology and vegetation productivity under climate extremes. Journal of Geophysical Research: Biogeosciences, 120(10), 2036-2052, doi:10.1002/2015JG003144.

Ma, X., Huete, A., Cleverly, J., Eamus, D., Chevallier, F., Joiner, J., & Xie, Z. (2016). Drought rapidly diminishes the large net CO 2 uptake in 2011 over semi-arid Australia. Scientific reports, 6, 37747, doi:10.1016/S0034-4257(03)00054-3.

Mpelasoka, F., Awange, J. L., & Zerihun, A. (2018). Influence of coupled ocean-atmosphere phenomena on the Greater Horn of Africa droughts and their implications. Science of the Total Environment, 610, 691-702, doi:10.1016/j.scitotenv.2017.08.109.

Murthy, C. S., Singh, J., Kumar, P., & Sai, M. S. (2016). Meteorological drought analysis over India using analytical framework on CPC rainfall time series. Natural Hazards, 81(1), 573-587.

Murthy, C. S., Singh, J., Kumar, P., & Sai, M. S. (2017). A composite index for drought hazard assessment using CPC rainfall time series data. International Journal of Environmental Science and Technology, 14(9), 1981-1988.

Newnham, G. J., Verbesselt, J., Grant, I. F., & Anderson, S. A. (2011). Relative Greenness Index for assessing curing of grassland fuel. Remote Sensing of Environment, 115(6), 1456-1463, doi:10.1016/j.rse.2011.02.005.

Pan, N., Feng, X., Fu, B., Wang, S., Ji, F., & Pan, S. (2018). Increasing global vegetation browning hidden in overall vegetation greening: Insights from time-varying trends. Remote Sensing of Environment, 214, 59-72, doi:10.1016/j.rse.2018.05.018.

Pandey, P. C., Mandal, V. P., Katiyar, S., Kumar, P., Tomar, V., Patairiya, S., & Gangwar, B. (2015). Geospatial approach to assess the impact of nutrients on Rice equivalent yield using MODIS sensors'-based MOD13Q1-NDVI Data. IEEE Sensors Journal, 15(11), 6108-6115.

Ponce-Campos, G. E., Moran, M. S., Huete, A., Zhang, Y., Bresloff, C., Huxman, T. E., & Scalley, T. H. (2013). Ecosystem resilience despite large-scale altered hydroclimatic conditions. Nature, 494(7437), 349-352, doi:10.1038/nature11836.

Rieser, D., Kuhn, M., Pail, R., Anjasmara, I. M., & Awange, J. (2010). Relation between GRACE-derived surface mass variations and precipitation over Australia. Australian Journal of Earth Sciences, 57(7), 887-900, doi:10.1080/08120099.2010.512645.

Rojas, O., Vrieling, A., & Rembold, F. (2011). Assessing drought probability for agricultural areas in Africa with coarse resolution remote sensing imagery. Remote sensing of Environment, 115(2), 343-352, doi:10.1016/j.rse.2010.09.006.

Tapley, B., Belabour, S., Watkins, M., Reigber, C., 2004. The gravity recovery and climate experiment: mission overview and early results. Geophys. Res. Lett. 31, 1–4. https://doi.org/10.1029/2004GL019920.

Tomar, V., Mandal, V. P., Srivastava, P., Patairiya, S., Singh, K., Ravisankar, N., & Kumar, P. (2014). Rice equivalent crop yield assessment using MODIS sensors' based MOD13A1-NDVI data. IEEE Sensors Journal, 14(10), 3599-3605.

Van Dijk, A. I., Beck, H. E., Crosbie, R. S., de Jeu, R. A., Liu, Y. Y., Podger, G. M., & Viney, N. R. (2013). The Millennium Drought in southeast Australia (2001–2009): Natural and human causes and implications for water resources, ecosystems, economy, and society. Water Resources Research, 49(2), 1040-1057, doi:10.1002/wrcr.20123.

Vousoughi, F. D., Dinpashoh, Y., Aalami, M. T., & Jhajharia, D. (2013). Trend analysis of groundwater using non-parametric methods (case study: Ardabil plain). Stochastic environmental research and risk assessment, 27(2), 547-559, doi:10.1007/s00477-012-0599-4.

Waring, R. H., Coops, N. C., Fan, W., & Nightingale, J. M. (2006). MODIS enhanced vegetation index predicts tree species richness across forested ecoregions in the contiguous USA. Remote Sensing of Environment, 103(2), 218-226, doi:10.1016/j.rse.2006.05.007.

Xiao, X., Boles, S., Liu, J., Zhuang, D., & Liu, M. (2002). Characterization of forest types in Northeastern China, using multi-temporal SPOT-4 VEGETATION sensor data. Remote Sensing of Environment, 82(2-3), 335-348, doi:10.1016/S0034-4257(02)00051-2.

Yadav, R., Tripathi, S. K., Pranuthi, G., & Dubey, S. K. (2014). Trend analysis by Mann-Kendall test for precipitation and temperature for thirteen districts of Uttarakhand. Journal of Agrometeorology, 16(2), 164.

Yang, Y., Long, D., Guan, H., Scanlon, B. R., Simmons, C. T., Jiang, L., & Xu, X. (2014). GRACE satellite observed hydrological controls on interannual and seasonal variability in surface greenness over mainland Australia. Journal of Geophysical Research: Biogeosciences, 119(12), 2245-2260, doi:10.1002/2014JG002670.

Zhang, X., Friedl, M. A., Schaaf, C. B., Strahler, A. H., Hodges, J. C., Gao, F., & Huete, A. (2003). Monitoring vegetation phenology using MODIS. Remote sensing of environment, 84(3), 471-475, doi:10.1016/S0034-4257(02)00135-9.

Zhang, X., Wang, J., Gao, F., Liu, Y., Schaaf, C., Friedl, M., & Yan, D. (2017). Exploration of scaling effects on coarse resolution land surface phenology. Remote Sensing of Environment, 190, 318-330, doi:10.1016/j.rse.2017.01.001.

Tao, F., Chen, Y., Fu, B. (2020). Impacts of climate and vegetation leaf area index changes on global terrestrial water storage from 2002 to 2016. Science of the total enviroment, 724, 138298, doi:/10.1016/j.scitotenv.2020.138298.

Ndehedehe, C.E., Ferreira, V.G., Agutu, N.O. (2019). Hydrological controls on surface vegetation dynamics over West and Central Africa. Ecological Indicators, 103, 494-508, doi:/10.1016/j.ecolind.2019.04.032.

Preisendorfer, R.(1988). Principal component analysis in meteorology and oceanography. Elsevier.